Journal of Materials Research and Technology 40 (2026) 2491–2502

Contents lists available at ScienceDirect

Journal of Materials Research and Technology

journal homepage: www.elsevier.com/locate/jmrt

Effects of heat-treatment temperature on the adhesive bonding performance of Ti–6Al–4V alloy

Yila Gaqi *, Shuqi Guo, Masahiro Kusano, Kimiyoshi Naito, Makoto Watanabe

Research Center for Structural Materials, National Institute for Materials Science, 1-2-1 Sengen, Tsukuba, 305-0047, Ibaraki, Japan

ARTICLE INFO

Keywords:
Titanium alloy adhesive bonding
Surface treatment
Heat treatment
Surface recontamination

ABSTRACT

In recent years, titanium alloys have been increasingly applied in the aerospace industry due to their low density, excellent mechanical properties, and corrosion resistance. Compared with bolting and welding, adhesive bonding offers advantages including reduced weight and more uniform stress distribution. In this work, a simple surface-activation method, namely electric-furnace heating at 200–800 °C for 1 h was evaluated to improve the adhesive bonding of ground Ti–6Al–4V sheets. Heat treatment produced a TiO_2-rich surface, reduced adventitious carbon, and increased wettability. The optimum condition was 400 °C for 1 h, which yielded the highest energy release rate (*Gc*) of 1455 J/m^2 in double cantilever beam (DCB) tests, with a predominantly cohesive failure mode (96 %). This was markedly higher than that of the as-ground surface, which exhibited a *Gc* of 924 J/m^2 and a cohesive failure proportion of only 46 %. At 800 °C, a thick Al_2O_3-containing layer formed and early delamination occurred at the brittle oxide/Ti–6Al–4V interface, driving *Gc* toward zero. After the treatment, the surface became recontaminated when the sheets were exposed to laboratory air above 48 h, resulting in hydrophobic recovery and a reduction in *Gc*. The comprehensive results indicate that an effective condition for Ti–6Al–4V is 400–600 °C for ~1 h in air, followed by immediate bonding before any recontamination.

1. Introduction

In the aviation industry, the lightweight design of aircraft components has been a key research focus, motivated by economic and environmental concerns to reduce fuel costs and carbon emissions [1,2]. Due to their excellent specific mechanical strength and corrosion resistance, titanium (Ti) alloys have been widely used as structural components, such as landing gear and hydraulic lines [1,3]. To assemble products from multiple titanium alloy components, bolting, riveting, and welding are commonly used. In contrast, adhesive bonding can be a promising alternative to conventional joining methods by offering a more lightweight design, minimizing the need for additional machining for bolts and rivets [4,5], and mitigating thermal deformation and property degradation caused by welding [6,7]. Accordingly, there is growing interest in multi-material bonding configurations that pair Ti with carbon fiber reinforced plastic (CFRP), aluminum (Al), or steel (i.e., Ti–CFRP, Ti–Al, and Ti–steel joints), as these architectures enable lightweight structures while leveraging the complementary properties of dissimilar constituents [8].

Despite these advantages, the adhesion of titanium alloys to polymer-based adhesives is generally low, reflecting weak interfacial bonding at the alloy–adhesive interface. This is primarily due to their chemically inert surfaces and low surface energy, which hinder effective chemical bonding and wetting with adhesives and lead to low bonding performance that must be overcome [9]. To address this challenge, various surface treatment strategies have been developed. Sanding with sandpaper and sandblasting is easy to perform and can provide micron-scale mechanical interlocking [10,11], but its performance improvements are limited, and they often need to be combined with other processes [12,13]. Chemical or electrochemical treatments (such as acid etching and anodizing) can significantly enhance bonding performance [13–16], but they involve the use of corrosive reagents and the disposal of waste liquids, which pose environmental burdens [13]. Laser surface treatment features high precision and good repeatability. It can generate roughened adherend surfaces that mechanically interlock with resin adhesives, thereby enhancing the bonding performance of titanium alloys [17–19]. However, the high capital cost of the equipment and the relatively low processing throughput limit its suitability for large-area or

* Corresponding author.
E-mail addresses: YILA.Gaqi@nims.go.jp (Y. Gaqi), GUO.Shuqi@nims.go.jp (S. Guo), KUSANO.Masahiro@nims.go.jp (M. Kusano), NAITO.Kimiyoshi@nims.go.jp (K. Naito), WATANABE.Makoto@nims.go.jp (M. Watanabe).

https://doi.org/10.1016/j.jmrt.2025.12.197
Received 5 October 2025; Received in revised form 15 December 2025; Accepted 19 December 2025
Available online 2 January 2026

high-throughput applications. In essence, these methods work by modifying surface topography (for mechanical interlocking and greater contact area) and by activating the surface (decontamination, higher surface energy/wettability, and introduction/exposure of reactive functional groups). Therefore, researchers are seeking more environmentally friendly, cost-effective, and easily implementable approaches to further improve the adhesive bonding performance of titanium alloys.

In contrast, titanium alloys used for implants sometimes undergo a deliberate surface oxidation treatment to remove adsorbed contaminants and thereby enhance biocompatibility [20,21]. For example, MacDonald et al. [22] found that heat treatment of Ti–6Al–4V at 600 °C for 1 h resulted in the formation of a thicker titanium oxide layer on the surface, significantly improved wettability, and promoted osteoblast adhesion. Similarly, García-Alonso et al. [23] showed that heating Ti–6Al–4V at 500 °C and 700 °C for 1 h resulted in the surface being composed predominantly of TiO_2 and a significant reduction of the C1s contamination peak, according to XPS analysis. They noted that heat treatment did not introduce new contaminants, indicating that high-temperature treatment effectively removes organic carbon from the surface. Additionally, Wang et al. [24] reported that heat oxidation of Ti–6Al–4V at 450 °C for 2 h markedly enhanced its surface hydrophilicity, as indicated by a static water contact angle of less than 10°. X-ray diffraction (XRD) analysis in their study revealed the presence of both anatase and rutile TiO_2 on the oxidized surface, which accompanied the improvement in wettability. These observations demonstrate that heat treatment can substantially improve the wettability of the Ti–6Al–4V surface, which is a promising indication for adhesive bonding.

In light of the above findings, heat treatment can be considered an economical and straightforward surface treatment that removes organic contaminants, increases surface energy (wettability), and introduces beneficial chemical functional groups, making it a promising option for the adhesive bonding of Ti–6Al–4V alloys. However, the distinct surface states of Ti–6Al–4V generated at different heat-treatment temperatures, as reflected in their chemical composition, oxide phase constitution, and oxide-layer thickness, may result in different adhesive bonding behaviour. In particular, at the early stages of oxidation, the originally formed sub-stoichiometric TiO and Ti_2O_3 species (Ti^{2+}/Ti^{3+}) are progressively converted into a predominantly TiO_2 (Ti^{4+}) surface as oxidation proceeds [25]. Among the various forms of TiO_2, an amorphous TiO_2 surface layer has been reported to form a “mixed interphase” with epoxy adhesives, providing abundant reaction sites for Ti–O–C bond formation and thereby significantly enhancing interfacial bonding strength [26]. By contrast, rutile-type crystalline TiO_2, which appears at temperatures above about 500 °C, can exhibit superhydrophilic behavior but is also accompanied by Al diffusion within the oxide scale, which is unfavorable for adhesive bonding [22,27]. At still higher temperatures (750–1000 °C), the Al content in the oxide scale increases sharply and the oxide film develops a porous and brittle morphology [27–29], which is generally considered detrimental to bonding.

In this study, we investigated the feasibility of thermal oxidation as a surface treatment for adhesive bonding of Ti–6Al–4V sheets. Treatment temperature was surveyed over a wide range of 200–800 °C, and the persistence of the surface-treatment effect under laboratory-air exposure was also evaluated. Adhesive bonding performance was quantified by the double cantilever beam (DCB) test for energy release rate Gc and the single-lap adhesive joint (SLAJ) test for shear strength τ. The influence of heat-treatment-induced surface modifications on bonding performance was elucidated through multi-scale characterization, including surface morphology and roughness, wettability, phase structure, and surface chemistry. Based on these results, we discuss the potential applicability of thermal oxidation as a surface treatment for adhesive bonding of titanium alloys.

2. Materials and methods

2.1. Evaluation method: DCB and SLAJ tests

The DCB test and SLAJ test were selected to evaluate the adhesive bonding performance of Ti–6Al–4V alloy sheets (90 mm × 25 mm × 3 mm, AMS 4911 R [30]; VSMPO-AVISMA Corporation). To ensure consistent surface conditions across all specimens, the adherends were ground using a surface grinding machine. An 80-grit silicon carbide grinding stone (Noritake GC80I; Noritake Co.) was operated at a speed of 2000 m/min, followed by final precision grinding with a feed rate of 0.2 μm per pass. After grinding, each specimen was ultrasonically cleaned in ethanol for 15 min and subsequently in acetone for another 15 min. Heat treatments were then carried out as described in Section 2.2.

For DCB specimens (Fig. 1), two Ti–6Al–4V sheets were bonded using two plies of epoxy film adhesive (FM309-1 M, Solvay; 90 mm × 25 mm each; total thickness of approximately 0.2 mm). A release film was inserted between the adhesive plies at one end to create an artificial pre-crack of 35 mm. Loading–hold–unloading tests were conducted on a tensile testing machine (Table-Top EZ-LX; Shimadzu Corp.) equipped with a 5 kN load cell, operating under displacement control at a crosshead speed of 1.0 mm/min at room temperature.

For SLAJ specimens (Fig. 2), the bonded overlap was 25 mm × 20 mm, and two plies of the same film adhesive used for the DCB specimens (25 mm × 20 mm) were applied. SLAJ tests were conducted at room temperature on a universal testing machine (AG-50kND; Shimadzu Corp.) under displacement control at a crosshead speed of 1.0 mm/min, and the maximum load was recorded. Shear strength τ was defined as the maximum load divided by the overlap area.

All assemblies were cured in an autoclave (Ashida Manufacturing Co.) at 180 °C and 0.28 MPa, according to the manufacturer's recommended curing conditions. For each surface treatment method, at least five specimens were prepared.

2.2. Surface treatment

Heat treatment was conducted using a muffle furnace (Computerized Furnace KDF 009G; Denken Co.) to modify the surface of Ti–6Al–4V specimens. The specimens were heated from room temperature to the target temperature at a rate of 30 °C/min, held at the target temperature for 1 h, and then cooled naturally to room temperature inside the furnace (furnace cooling). Guided by the temperature-dependent oxidation behaviour of Ti–6Al–4V described in the Introduction, the heat-treatment temperatures (T) were set to 200, 300, 400, 500, 600, and 800 °C to identify an optimal processing temperature window. This matrix covers a low-temperature regime (200–300 °C), below the reported onset of anatase crystallization (~276 °C [31]), where only limited modification of the native amorphous oxide and partial surface decontamination are expected; an intermediate regime (400–600 °C), where previous studies have shown significant thickening and crystallization of the TiO_2 scale into anatase/rutile [22–24]; and a high-temperature point (800 °C), within the range where over-oxidation, Al_2O_3 enrichment, and oxide-scale spallation have been reported for Ti–6Al–4V [27–29], while all selected temperatures remain below the β-transus of Ti–6Al–4V [32].

2.3. Surface observation

The surface morphology of the heated Ti–6Al–4V specimens was observed using an optical microscope (OM, VHX-7100; Keyence) and a scanning electron microscope (SEM) (JSM-6010LA; JEOL). Elemental distribution on the heated surfaces was analyzed by energy-dispersive X-ray spectrometry (EDS) with an EDS detector in the SEM. Surface roughness parameters (R_a and R_z) were measured using VHX software based on height profile analysis.

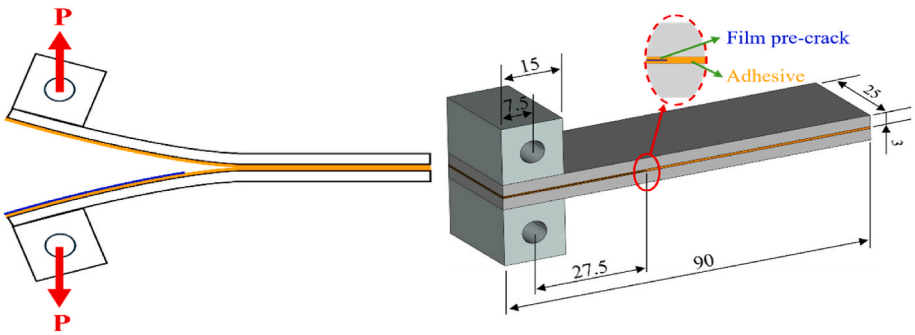

Fig. 1. Schematic illustration of the DCB specimen geometry (unit: mm).

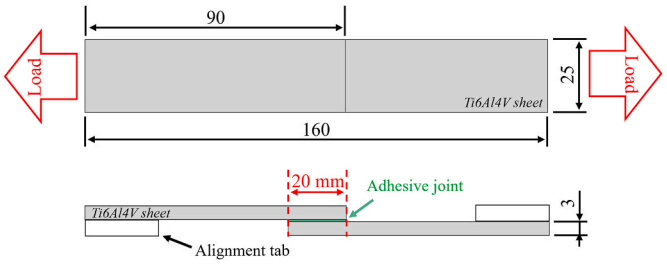

Fig. 2. Schematic illustration of the SLAJ specimen geometry (unit: mm).

Wettability was evaluated by measuring the static contact angle of pure water using a contact angle meter (DMo-602; KYOWA Science Co.). The droplet volume was fixed at 1.5 μL, and measurements were taken 2000 ms after drop deposition. All contact angle measurements were performed within 30 min after removal from the furnace to minimize the influence of surface recontamination. The phase composition and crystal structure of the heated specimen surfaces were characterized by glancing angle X-ray diffraction (GI-XRD; SmartLab, Rigaku, Japan) using Cu Kα radiation (wavelength $\lambda = 1.5418$ Å, 45 kV and 200 mA), with a scan rate of 0.4005°/min over a diffraction angle 2θ range of 5°–120°. The incident angle was set to 0.3°. Surface chemical composition and oxidation states were analyzed by XPS (Quantera SXM, ULVAC-PHI, Japan) using a scanning monochromatic Al Kα source (energy resolution <0.5 eV).

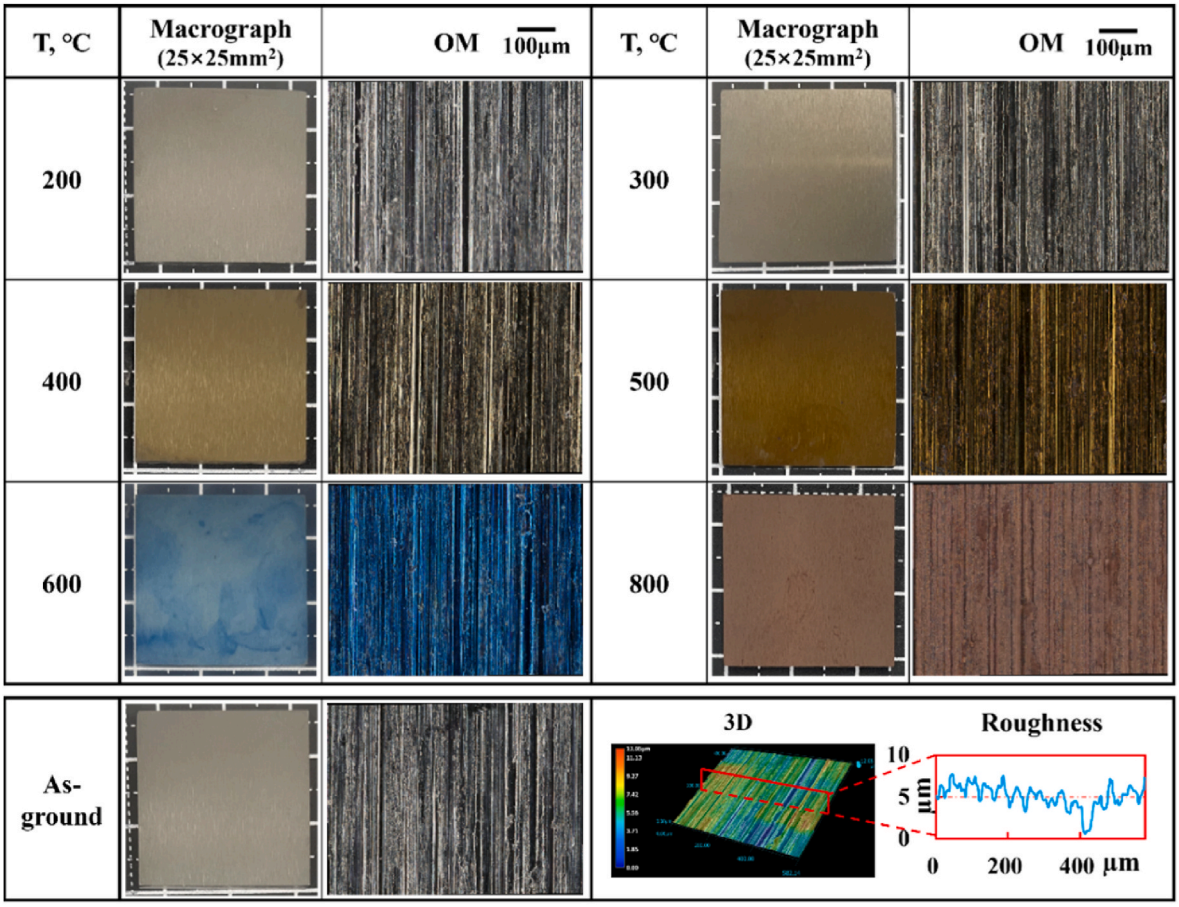

Fig. 3. Macrograph and optical microscope (OM) images of Ti–6Al–4V surfaces heated at different temperatures for 1 h. The bottom row shows the as-ground surface and a schematic of the roughness measurement method.

3. Results and discussion

3.1. Surface morphology and structural analysis

Fig. 3 shows macrograph and OM images of the Ti–6Al–4V surfaces after heat treatment at various temperatures (200–800 °C) for 1 h. To facilitate comparison, the bottom of Fig. 3 includes both the images of the unheated specimen and a schematic illustration of the surface roughness measurement method. The corresponding surface roughness results are presented in Fig. 4. These values represent the average of ten randomly selected measurements. With increasing heat-treatment temperature, noticeable changes in surface color were observed. However, at 2000 × magnification, the arithmetic average roughness R_a remained around 1.0 μm, and even the average maximum peak-to-valley height R_z stayed within 10–15 μm, showing no appreciable change. Beginning at 200 °C, the silver surface color gradually changed from light yellow to deeper tones with increasing temperature, becoming distinctly yellow-brown at 500 °C. At 600 °C, the surface turned blue, and further heat treatment at 800 °C resulted in a dark brown surface. According to the findings of Diamanti et al. [33], the observed surface color changes are primarily attributable to variations in thin-film optical interference caused by the increasing thickness. To validate this interpretation, cross-sectional SEM and EDS-mapping analyses were conducted on specimens heated at different temperatures. Fig. 5(a) shows representative cross-sectional SEM and EDS images after heat treatment. The oxide-layer thickness clearly increases with temperature, from <1 μm to about 10 μm. This trend correlates well with the gradual surface color transition described earlier—from light yellow at lower temperatures to yellow-brown, blue, and finally dark brown at higher temperatures.

Additionally, the EDS mapping element maps at 800 °C, as shown in Fig. 5 (b), further reveal pronounced element diffusion at 800 °C. The oxide layer consists of an Al_2O_3-rich outer layer and a TiO_2-rich inner layer, with trace vanadium (V)-containing oxide species distributed throughout. These observations indicate that high-temperature exposure promotes outward diffusion of Al and, to a lesser extent, V [20]. Although such secondary oxides (e.g., Al- and V-containing oxides) can influence the optical response, their contribution to color formation is generally minor compared with the dominant interference effect governed by film thickness [34].

As reported by Melo Rodriguez et al. [34], with increasing heat-treatment temperature, the TiO_2 film undergoes a phase transformation from an amorphous or anatase phase to the rutile phase. This change in microstructure, including crystal structure and crystallographic orientation, can also lead to local variations in oxide thickness and porosity. This results in subtle color differences across the surface. GI-XRD analysis was conducted on specimens heated at different temperatures to examine these structural changes. As shown in Fig. 6(a), the GI-XRD patterns revealed distinct changes in surface phase composition

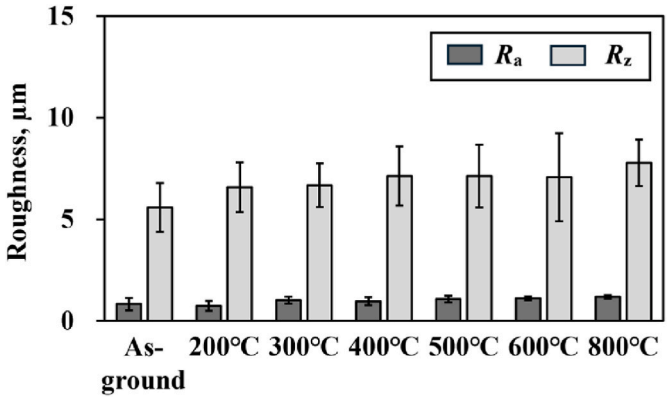

Fig. 4. Surface roughness parameters (R_a and R_z) of Ti–6Al–4V specimens heated at various temperatures.

with increasing heat-treatment temperature. In the 200–400 °C range, no clear TiO_2 diffraction peaks were observed, even though GI-XRD, which offers improved surface sensitivity, was employed. Combined with EDS results, this suggests that the oxide films formed at these temperatures are extremely thin and possess very low crystallinity, or amorphous phase.

The incident X-rays can easily penetrate such thin films and are predominantly diffracted by the underlying α-Ti substrate, while the strong substrate signals may overshadow any weak response from the oxide layer. This observation is also consistent with previous reports [35,36], which noted the difficulty of detecting ultrathin oxide films using conventional XRD techniques.

At 500 °C, weak diffraction features begin to appear in the low-2θ region (see the magnified inset in Fig. 6), suggesting the incipient crystallization of surface oxides. Consistent with this finding, Wang et al. reported the simultaneous presence of anatase and rutile after heat treatment at 450 °C for 2 h [24]. From 600 °C onward, distinct rutile--TiO_2 peaks intensify, confirming the formation of a crystalline oxide layer. At 800 °C, the α-Ti peaks almost completely vanish, indicating a sufficiently thick oxide layer capable of blocking or overwhelming the diffraction from the substrate. Mass-fraction analysis of the 800 °C-1 h oxide layer, performed in PDXL2 (Rigaku, Japan) using the reference-intensity-ratio method, indicates that the diffraction pattern is dominated by rutile TiO_2 (64.7 ± 0.6 wt%), with secondary Al_2O_3 (32.0 ± 0.6 wt%). In this study, although V_2O_3 reflections were not prominent in the 800 °C pattern, quantitative XRD analysis indicated 3.3 ± 0.4 mass % V_2O_3. This is in line with the reports of MacDonald et al. [22] and Melo Rodriguez et al. [20], who observed outward diffusion of Al to the surface as Al_2O_3—an effect that becomes more pronounced with increasing treatment temperature; analogous behavior is also noted for V. At 600 °C, outward diffusion of Al and V was not evident in the EDS scans, most likely because their contents in the oxide layer were much lower than in the 800 °C specimen. By contrast, clear Al enrichment was captured by EDS after heat treatment at 800 °C, consistent with the phase evolution indicated by XRD.

Moreover, with increasing heat-treatment temperature, the α-Ti diffraction peaks gradually shift toward lower 2θ angles. Valentine et al. [37] reported a similar shift during in-situ heating of Ti–6Al–4V powders and related it to lattice expansion. In our ex-situ, room-temperature measurements, the accompanying increase in unit-cell volume V (Fig. 6 (b)) likewise indicates an expansion of the α-Ti lattice, which can be ascribed primarily to oxygen uptake and microstructural relaxation during oxidation. This interpretation is further supported by the evolution of lattice strain shown in Fig. 6(c): the lattice strain remains relatively high (about 1.3–1.5 %) in the 200–400 °C range, but exhibits a marked decrease starting from 500 °C. Such a reduction in lattice strain suggests the onset of stress relaxation at elevated temperatures, which aligns with the findings of Guleryuz et al. [28], who reported that above 500 °C the growth of a thicker and more compact oxide scale promotes the release of surface residual stress. In addition, oxygen diffusion into the substrate tends to stabilize, thereby reducing lattice distortion. However, no diffraction peaks corresponding to β-Ti were detected in any of the samples. According to the AMS 4911 R standard [30], the alloy typically contains a small amount of β phase in addition to the dominant α phase. The absence of β-Ti peaks may be due to its very low volume fraction falling below the detection limit of conventional XRD [38].

3.2. XPS results

The XPS analysis was conducted on the untreated sample ("as-ground") and samples heated at 200 °C, 400 °C, 600 °C, and 800 °C. The results are given in Fig. 7 (Shift C1s 284.60 eV).

As shown in the four spectra in Fig. 7, the O 1s, Ti 2p, and Al 2p peak shapes and intensities for the sample heated at 200 °C for 1 h (hereafter referred to as the 200°C–1h sample) remain largely unchanged

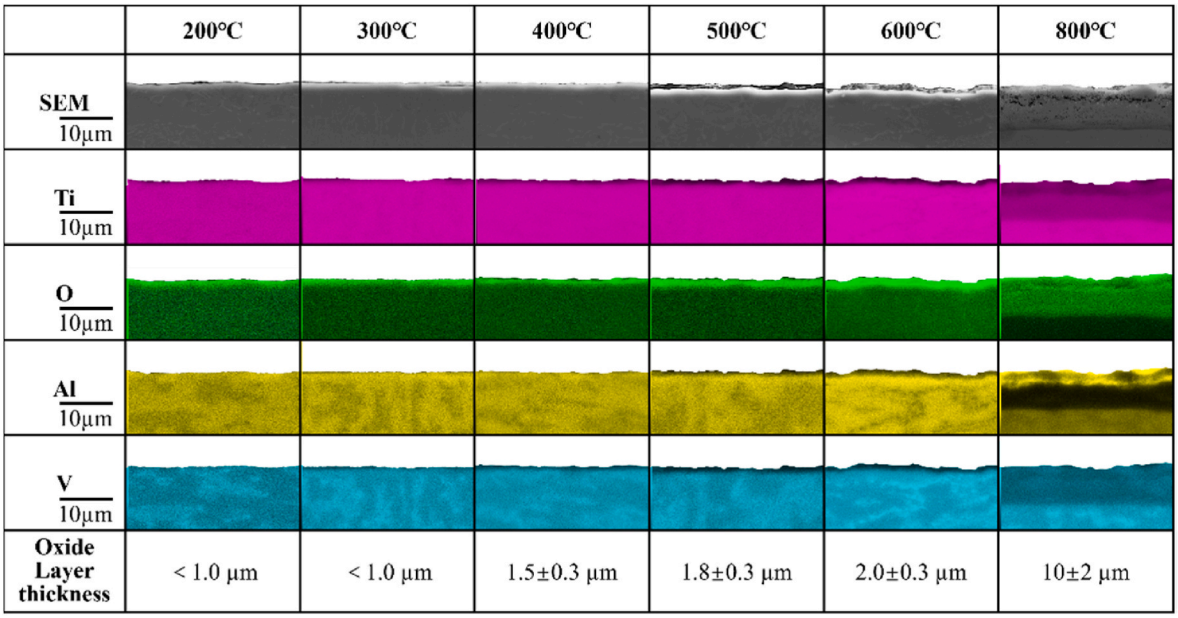

Fig. 5(a). Cross-sectional SEM, EDS images, and oxide layer thickness of Ti–6Al–4V heated at different temperatures.

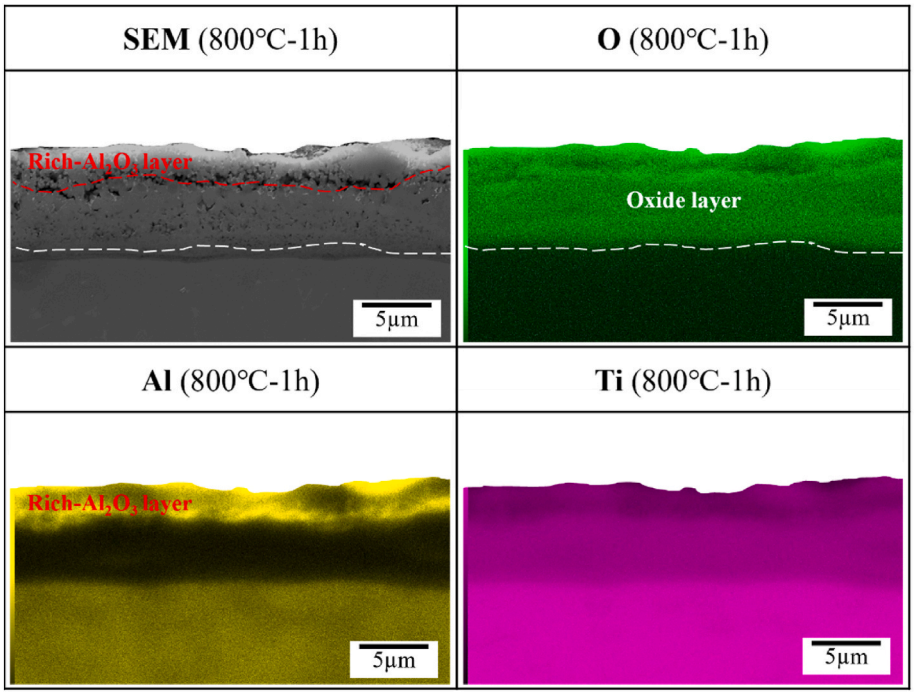

Fig. 5(b). Cross-sectional SEM, EDS images of Ti–6Al–4V heated at 800 °C for 1h.

compared with those of the untreated surface, especially in contrast to the spectra obtained at higher temperatures. This indicates that the surface chemistry undergoes little alteration at this stage. However, deconvolution of the Ti 2p spectra from the untreated (Fig. 8(a)) and 200°C–1h (Fig. 8(b)) samples reveals a key change: the Ti^{3+} components (associated with suboxides such as Ti_2O_3), which are clearly present in the untreated sample, disappear after heating, leaving only Ti^{4+} peaks characteristic of TiO_2. This observation aligns with the findings of Hierro-Oliva et al. [25], who performed in-situ XPS analysis of Ti–6Al–4V under low-oxygen conditions and found that initial oxide layers predominantly contained low-valence species (Ti^{2+}, Ti^{3+}), which gradually converted to fully oxidized TiO_2 with prolonged exposure or mild heating. Similarly, Carley et al. [39] reported that ultrathin oxide layers formed at room temperature in ambient air exhibited Ti^{2+} and Ti^{3+} features, whereas thicker oxide films generated by thermal oxidation showed predominantly Ti^{4+}. These findings suggest a thermodynamically driven oxidation pathway, whereby metastable Ti^{3+}-containing suboxides are further oxidized to TiO_2, resulting in the progressive replacement of Ti^{3+} by Ti^{4+} and the formation of a more stable, fully oxidized surface. In parallel, the C 1s signal decreases progressively with increasing heat-treatment temperature, beginning at 200 °C. This trend indicates the effective removal of adventitious carbon species and a cleaner surface state [23,24]. Therefore, even at relatively low temperatures, heat treatment can promote decontamination of the

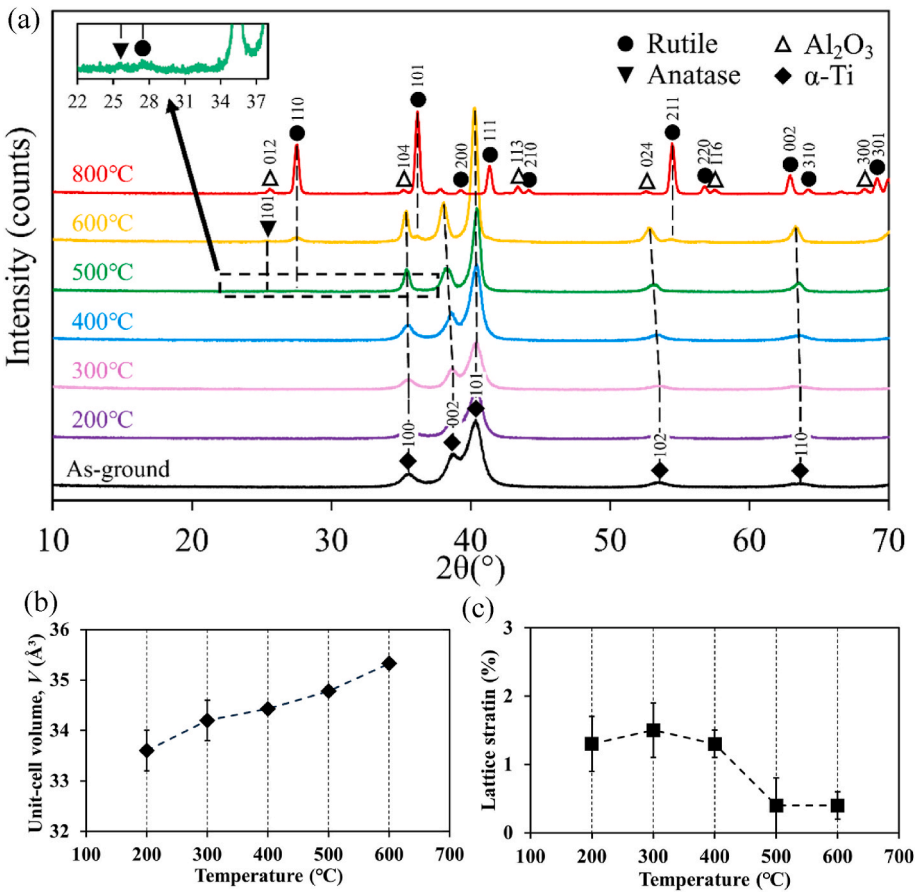

Fig. 6. (a) GI-XRD patterns, (b) α-Ti unit-cell volume, (c) lattice strain in α-Ti of Ti–6Al–4V samples after heat treatment at various temperatures.

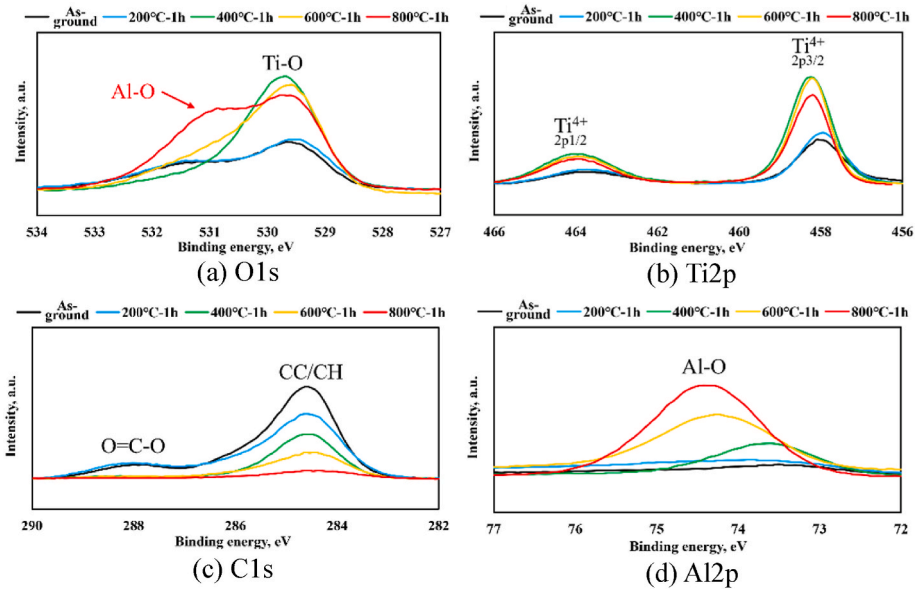

Fig. 7. XPS spectra of Ti–6Al–4V after heat treatment: (a) O1s; (b) Ti2p; (c) C1s; (d) Al2p (Shift C1s 284.60eV).

surface, although substantial oxide growth and chemical reconstruction have not yet occurred.

When the temperature is raised to 400 °C and 600 °C, in contrast to the surfaces of the untreated and the 200°C-1h samples, the O1s, Ti2p, and Al2p spectral peak intensities increase significantly, and the C1s peak intensity decreases markedly. In this mid-temperature range, an oxide layer dominated by Ti–O forms and begins to crystallize; this is in line with reports that amorphous/anatase titania on titanium alloys crystallizes and the rutile phase emerges around ~600 °C, depending on processing [20]. Between 400 °C and 600 °C, the O1s and Ti2p peak profiles and intensities show no obvious differences, but the Al2p peak intensity at 600 °C is slightly higher than that at 400 °C, and it increases

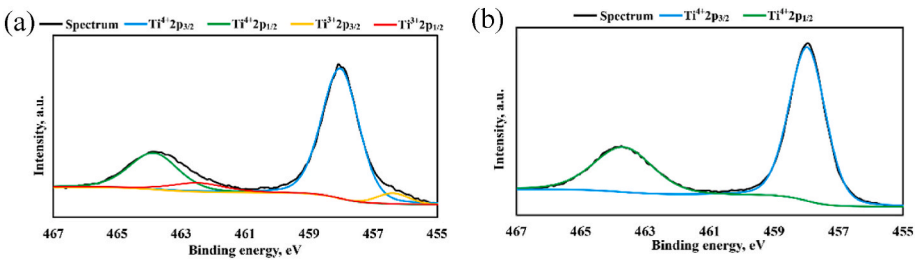

Fig. 8. XPS peak deconvolution of Ti2p spectra for (a) As-ground and (b) 200 °C-1 h samples.

further at 800 °C. This corresponds to the reports of temperature-driven Al enrichment in the outer oxide (Al_2O_3 contribution) [20,27].

At temperatures of 600–800 °C, as the Al2p signal continues to grow, the peak heights of Ti2p and O1s at 800 °C become lower than those at 600 °C. This behavior is readily explained by the outermost oxide becoming thicker and richer in Al_2O_3. The increased Al–O fraction within the overall O1s envelope reduces the relative contribution (and apparent peak height) of Ti–O, despite there being a higher total oxygen content. This evolution accompanies the rutile-dominated oxide layer reported at ≥600 °C on Ti–6Al–4V [20,40]. In addition, with increasing temperature, the Ti2p peak (especially the $Ti2p_3/_2$ peak) shows a modest positive chemical shift and sharpening, consistent with increased Ti^{4+} content, reduced defect states, and improved crystallinity of the oxide film; together with the XRD results, this supports the formation of a rutile-dominated TiO_2 layer at elevated temperatures.

3.3. Wettability

Fig. 9 illustrates the variation in contact angle of Ti–6Al–4V specimens heated at different temperatures for 1 h. The contact angle remained relatively high (~75°) up to 300 °C, indicating that wettability improvement was limited at lower heat-treatment temperatures. At ≥400 °C, however, the contact angle decreased sharply; at ≥500 °C it approached zero, which is characteristic of superhydrophilic behavior. A similar phenomenon was reported by Wang et al. [24], who found that Ti–6Al–4V heated at 450 °C exhibited superhydrophilicity with contact angles below 10°. The oxide layer formed at this temperature consisted of both anatase and rutile phases. In addition, Masahashi et al. [41] demonstrated that rutile-phase TiO_2, formed by anodic oxidation followed by high-temperature treatment, can also display near-zero contact angles even in the absence of UV activation. They attributed this behavior to the material's inherently high surface energy and nanostructured morphology.

Therefore, together with the XRD/XPS evidence, these results suggest that thermal treatment enhances wettability (i.e., surface energy) by forming a stable, low-defect TiO_2 surface on Ti–6Al–4V and by removing adventitious contaminants. This macroscopic increase in wettability is typically indicative of improved interfacial adhesion performance; accordingly, enhanced interfacial adhesion can be expected. However, some researchers [42] have pointed out that when titanium alloy surfaces undergo high-temperature air oxidation (above 400 °C), resulting in the formation of a relatively thick and crystalline TiO_2 layer, the adhesive strength may actually deteriorate. This is attributed to the potential formation of a weak interface between the adhesive and the dense, crystalline oxide layer, which can compromise bonding performance. These findings underscore the need to define a suitable thermal treatment window that balances surface activation with interfacial integrity for reliable adhesive bonding.

3.4. DCB test results

Load–displacement data from the DCB tests were used to calculate the crack stabilization *Gc* within the recommended crack length range (≤60 mm) according to ISO 25217. The average *Gc* values for each group are plotted in Fig. 10.

As shown, heat treatment at 200 °C for 1 h had little effect on the bonding performance. From 300 °C to 600 °C, significant improvement was observed, with all samples exhibiting *Gc* values exceeding 1300 J/m^2. The maximum *Gc* was recorded at 400 °C, reaching a peak *Gc* of 1455 J/m^2. However, at 800 °C, crack propagation occurred along the oxide layer, and the measured *Gc* sharply dropped to 6 J/m^2, indicating excessive oxidation.

Fig. 11 shows the specimen with the cohesive-failure area fraction closest to its group average under each condition. In the figure, exposed Ti–6Al–4V/adhesive interfaces are classified as adhesive failures (green dots) or cohesive failures (red dots). The as-ground and 200 °C specimens exhibit extensive interfacial exposure, while the 300–600 °C specimens show markedly less such exposure. Notably, the 400 °C condition displays almost 100 % cohesive failure. In addition, the cohesive-failure area fraction on each fracture surface was quantified, and the mean value for each condition is summarized in Fig. 12. It can be

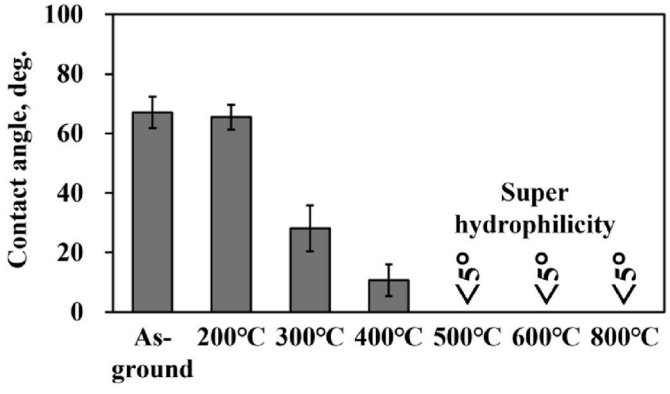

Fig. 9. Contact angle of Ti–6Al–4V specimens heated at different temperatures, measured within 30 min after removal from the furnace.

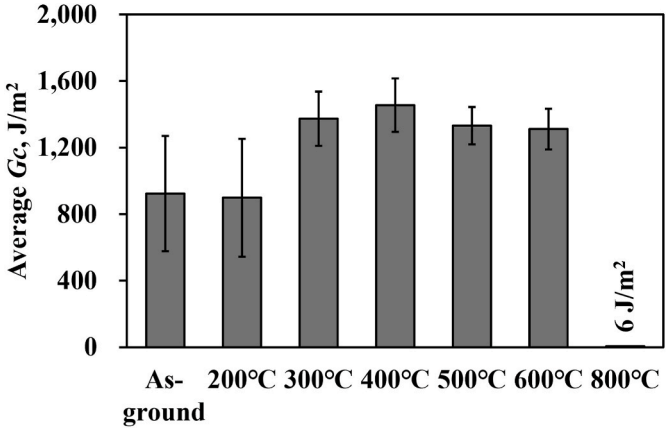

Fig. 10. Average *Gc* of DCB specimens heated at different temperatures for 1 h.

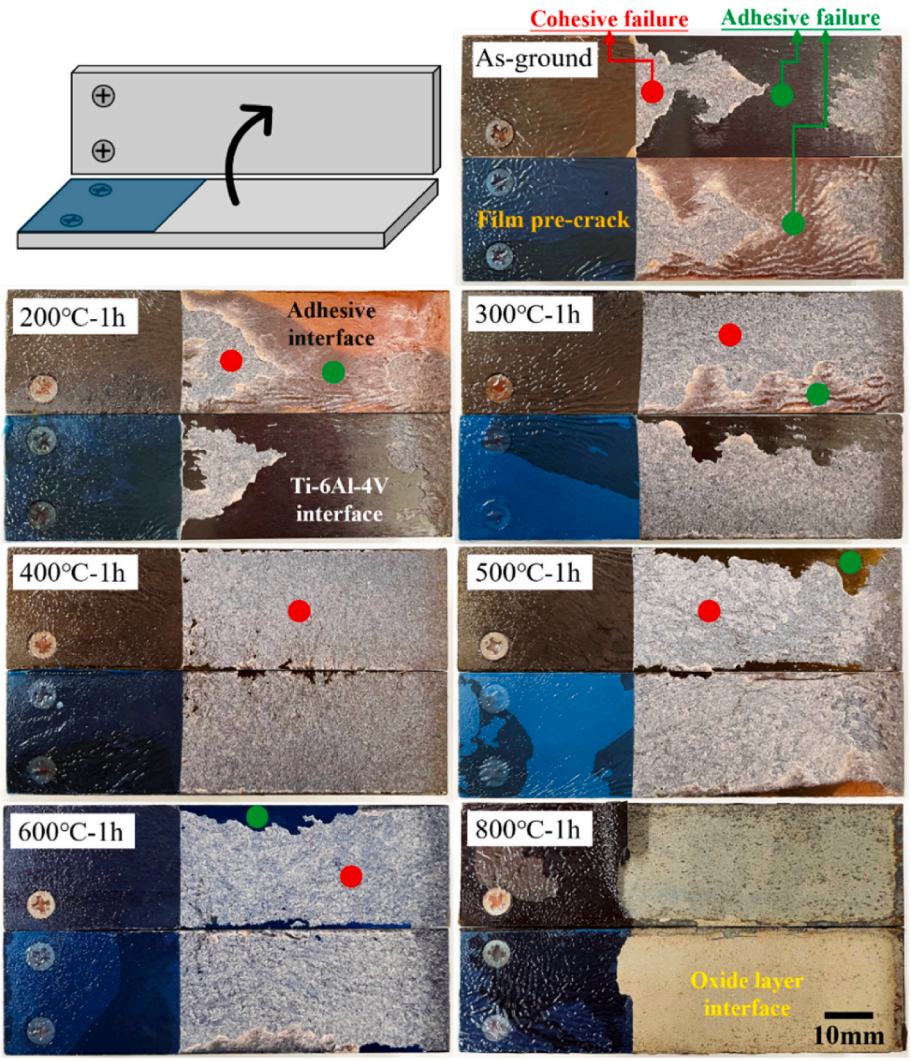

Fig. 11. Representative DCB fracture surfaces for each heat-treatment condition (specimens chosen to have a cohesive-failure area fraction closest to the group mean).

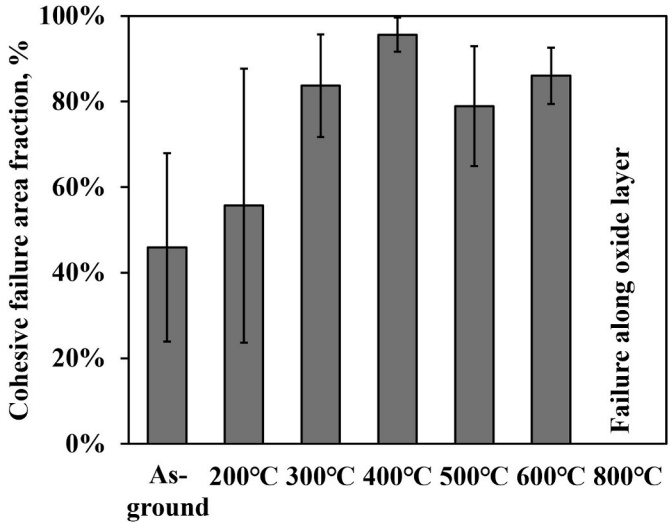

Fig. 12. Cohesive-failure area fraction under different heat-treatment temperatures.

seen that the cohesive-failure area fraction varies with temperature in a manner consistent with the average *Gc*. In particular, the 400 °C condition exhibits the highest cohesive fraction and the smallest scatter, indicating a more stable interface and a cohesion-dominated fracture behavior.

As mentioned in the introduction, the improvement of bonding performance for titanium alloys mainly relies on altering the surface morphology and activating the surface. Changing the surface morphology (by roughening the surface) creates more mechanical interlocking between the adhesive and the substrate, and increases the contact area, thereby enhancing the bonding performance. In this study, heating Ti–6Al–4V for 1 h at various temperatures did not produce a significant change in surface roughness; therefore, roughness was considered to make little or no contribution to the observed improvement in bonding performance. Instead, the enhancement was primarily attributed to surface activation, achieved through the removal of surface contaminants and the increase in surface energy [41].

Based on the above surface characterization results, it can be concluded that at lower temperatures, heat treatment primarily induces limited surface decontamination and activation, while the surface oxide layer remains largely in a low-crystallinity state. This level of activation is insufficient to significantly improve interfacial adhesion, which explains why the sample treated at 200 °C did not exhibit enhanced bonding strength. However, samples treated at 300 °C and 400 °C, which also retained low crystallinity, demonstrated relatively higher

bonding strength due to further improvements in surface cleanliness.

When the temperature increases to the intermediate range of 400–600 °C, Ti–O oxides begin to crystallize, the C 1s signal continues to decrease, and the density of polar surface active sites increases markedly. Meanwhile, Al surface enrichment remains limited (becoming significant only near 600 °C). Within this temperature window, the surface oxide layer possesses Ti–O features, moderate thickness, and high surface energy—conditions favorable for enhanced interfacial adhesion. Notably, the sample treated at 400 °C exhibited even higher bonding strength than those treated at 500 °C and 600 °C, despite having a lower degree of oxide crystallinity. A similar interfacial structure and bonding mechanism was reported by Li et al. [26], who used transmission electron microscopy (TEM) to observe the formation of an amorphous TiO_2 nano-oxide layer on laser-treated titanium alloy surfaces. This layer exhibited high permeability, allowing the epoxy adhesive to infiltrate and form a ~180 nm-thick interfacial "mixed layer" between the metal and adhesive. This structure provided abundant reaction sites for the formation of Ti–O–C chemical bonds, significantly enhancing interfacial bonding strength. Further molecular simulations revealed that the reaction barrier for Ti–O–C bond formation is low, enabling the reaction to proceed spontaneously during adhesive curing. Such chemical bonding is difficult to achieve, or only occurs locally, on more densely crystallized TiO_2 surfaces. At a higher temperature of 800 °C, the oxide layer becomes thicker and exhibits evident Al enrichment, leading to the formation of a brittle, Al-rich oxide scale. Crack propagation is then confined within the oxide layer itself, resulting in a characteristic cohesive failure mode that undermines the overall joint strength.

Moreover, no diffraction peaks corresponding to β-Ti were detected for any of the heat-treatment conditions. This supports the view that the changes induced by the present heat treatments are essentially confined to the near-surface region (oxide scale and oxygen-enriched layer), rather than involving a change in the bulk phase constitution. Since adhesive performance is governed mainly by the surface condition and the adhesive/substrate interface, the variations in bonding strength observed in this study are therefore attributed to heat-induced modifications of the surface oxide layer and interfacial chemistry, rather than to phase changes in the Ti–6Al–4V substrate.

Through the combined use of mechanical testing and multi-scale surface characterization, this study has preliminarily elucidated the key mechanisms by which heat treatment enhances the adhesive bonding strength of Ti–6Al–4V alloy. Nevertheless, further investigation is needed to clarify the specific influence of amorphous TiO_2 surface structures on adhesion behavior—particularly under low-temperature treatment—by employing higher-resolution techniques such as TEM in future work.

3.5. SLAJ test results

The τ obtained from the SLAJ tests is shown in Fig. 13. Compared with the as-ground (25.17 ± 1.9 MPa), heat treatment at 200 °C for 1 h (24.51 ± 2.1 MPa) had little effect on τ. In the 300–600 °C range, τ increased only modestly, by about 4–7 % (26.2–26.9 MPa). As also observed in the SLAJ tests, at 800 °C, failure occurred within the thick oxide layer, and the measured τ dropped to 3.3 MPa, indicating excessive oxidation.

Fig. 14 presents typical fracture surfaces of SLAJ specimens heated at different temperatures for 1 h. In the SLAJ test, the two edges of the adhesive layer along the loading direction (hereafter “adhesive edges”) are the regions of highest stress concentration, and the measured τ is largely governed by the bonding quality at these edges. At the adhesive edges, the as-ground and 200 °C specimens exhibit extensive adhesive failure. By contrast, after the 300–600 °C treatments, adhesive failure at the edges is confined to a narrow zone, suggesting improved interfacial adhesion performance. For the shear strength, although interfacial failure along the adhesive edges is clearly reduced at 300–600 °C

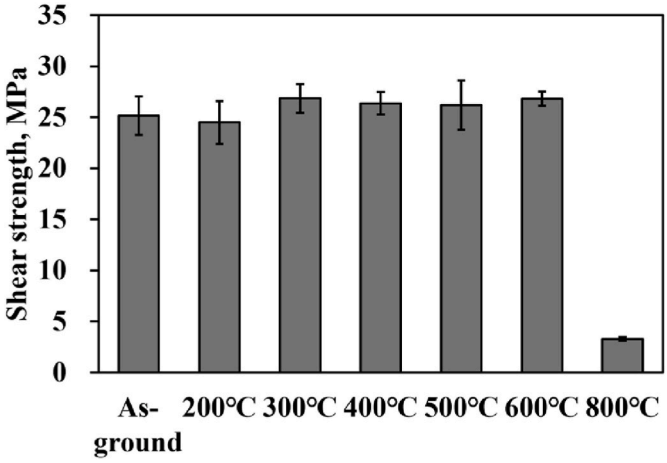

Fig. 13. Shear strength of SLAJ specimens heated at different temperatures for 1 h.

compared with the as-ground and 200 °C conditions, indicating an interfacial performance improvement, the measured τ increases only modestly. This likely reflects that SLAJ-measured shear strength is a structure-dominated metric controlled by peel/edge effects rather than a purely interfacial property. In addition to interfacial quality, shear strength is sensitive to adhesive thickness control and other geometric/processing factors. These influences should be verified in future work.

3.6. Effect of surface recontamination

Surface recontamination of titanium alloys has long been a critical issue for both adhesion and biomedical performance [43]. Although TiO_2 is intrinsically hydrophilic, its hydrophilicity decays with air exposure over time [44]. It is therefore necessary to evaluate the recontamination behavior of heated specimens under different storage conditions to inform practical processing.

Fig. 15 presents the static water contact angles of specimens heated at 400 °C for 1 h (after cooling), then either stored in the laboratory environment or left in the unopened furnace after cooling. The hollow and solid bars denote the baseline values of the as-ground (untreated) and 400°C–1h specimens from Fig. 9, respectively; each specimen was measured once and not reused. The results show that specimens stored in the laboratory exhibit a pronounced rebound in contact angle, nearly returning to the untreated level, whereas those kept inside the furnace retain essentially unchanged contact angles, indicating that hydrophilicity can be effectively maintained.

To relate wettability to interfacial performance and surface chemistry, specimens stored under the two conditions for 48 h were analyzed by DCB testing for *Gc* and by XPS (Figs. 16 and 17). The *Gc* of the furnace-held specimens after 48 h was slightly lower than that under the 400°C–1h condition but comparable to that under the 500°C–1h condition, whereas the laboratory-stored specimens showed a marked decrease in *Gc*, falling within the scatter of the as-ground condition. XPS revealed that the O1s, Ti2p, and Al2p peak shapes and intensities of furnace-held specimens remained essentially unchanged, suggesting a stable surface chemical state; in contrast, the laboratory-stored specimens displayed a renewed rise in C1s (adventitious carbon) toward the untreated level, although other elemental signals remained higher than those of the untreated surface. This recontamination explains the observed increase in contact angle and the concomitant decline in *Gc*.

In summary, when a delay before bonding is unavoidable, heated specimens should be kept inside the heat-treatment furnace without removing the samples or opening the chamber—i.e., in a sealed, clean, and relatively dry environment—to avoid exposure to ambient air and consequent contamination. Such in-furnace storage effectively

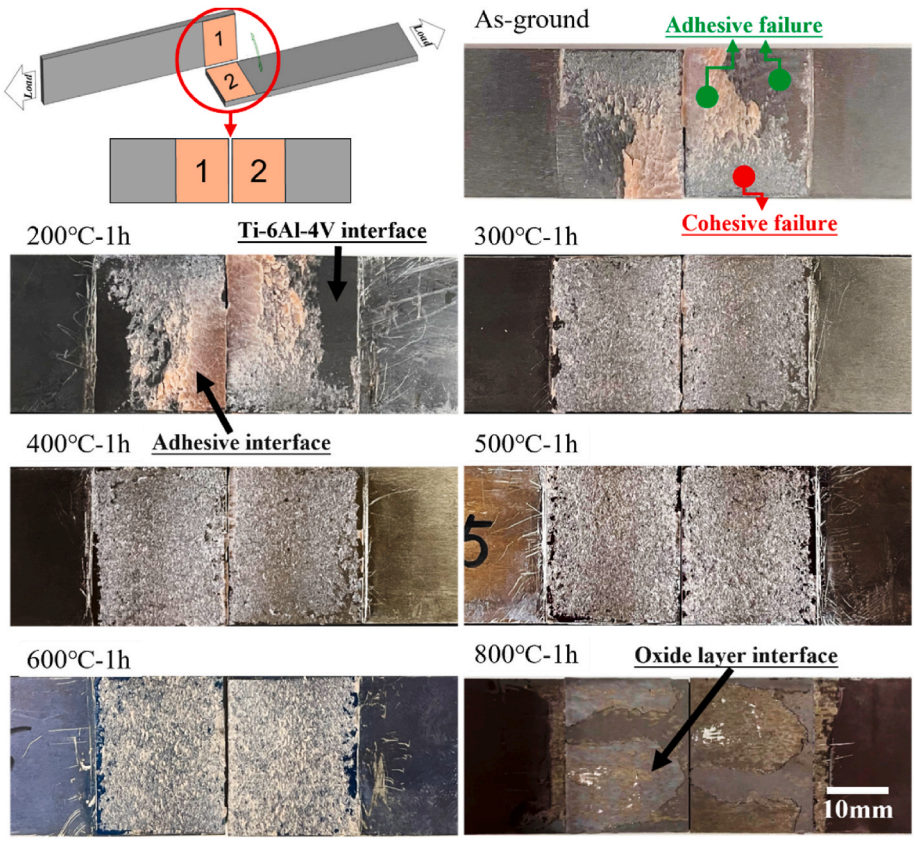

Fig. 14. Representative SLAJ fracture surfaces for each heat-treatment condition, selected to illustrate typical failure morphologies (adhesive, cohesive, or oxide layer-interface).

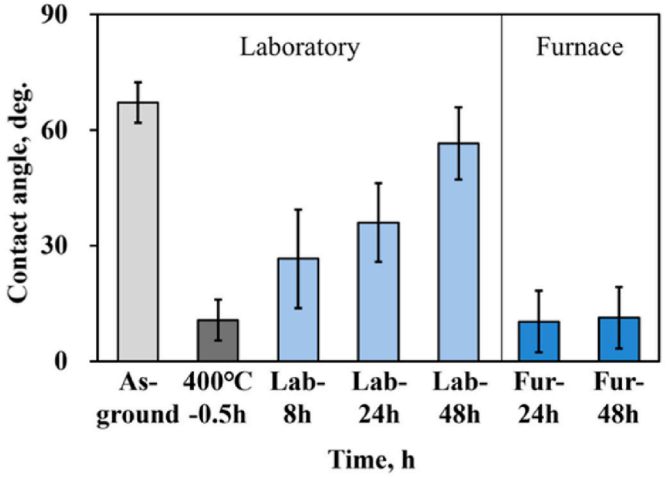

Fig. 15. Static water contact angle of Ti–6Al–4V heated at 400 °C for 1 h after storage in laboratory air vs. in-furnace (unopened).

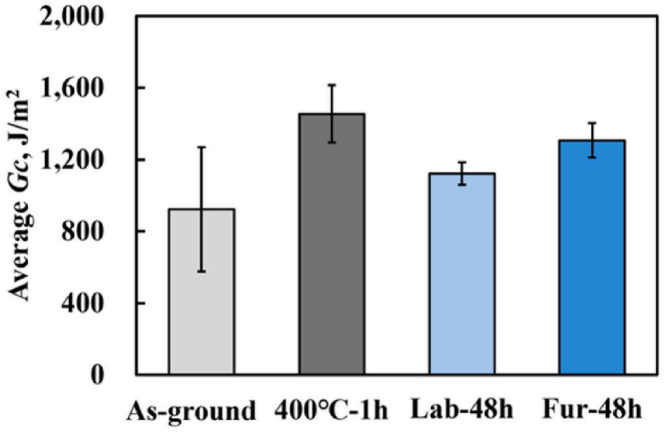

Fig. 16. Effect of 48 h storage on *Gc* (by DCB test) for Ti–6Al–4V heated at 400 °C for 1 h: laboratory air vs. in-furnace (unopened).

suppresses Such storage effectively suppresses air-induced re-adsorption of adventitious carbon and related surface recontamination, thereby maintaining hydrophilicity and bonding performance. By contrast, exposure to ordinary laboratory air rapidly induces surface recontamination, degrading both wettability and the interfacial energy release rate.

4. Conclusion

This study systematically evaluated the effect of heat treatment on the adhesive performance of Ti–6Al–4V to discuss the feasibility of thermal oxidation as a surface treatment. By combining DCB testing with multi-scale characterization (contact angle, OM/SEM, GI-XRD, XPS/EDS), the underlying mechanisms and processing window were elucidated. The main conclusions are as follows:

(1) The temperature-induced increase in bonding performance arises primarily from surface activation—namely, the removal of adventitious carbon (decrease in C1s) and other contaminants, the formation of a Ti–O-dominated oxide surface, and a marked increase in surface energy/wettability.

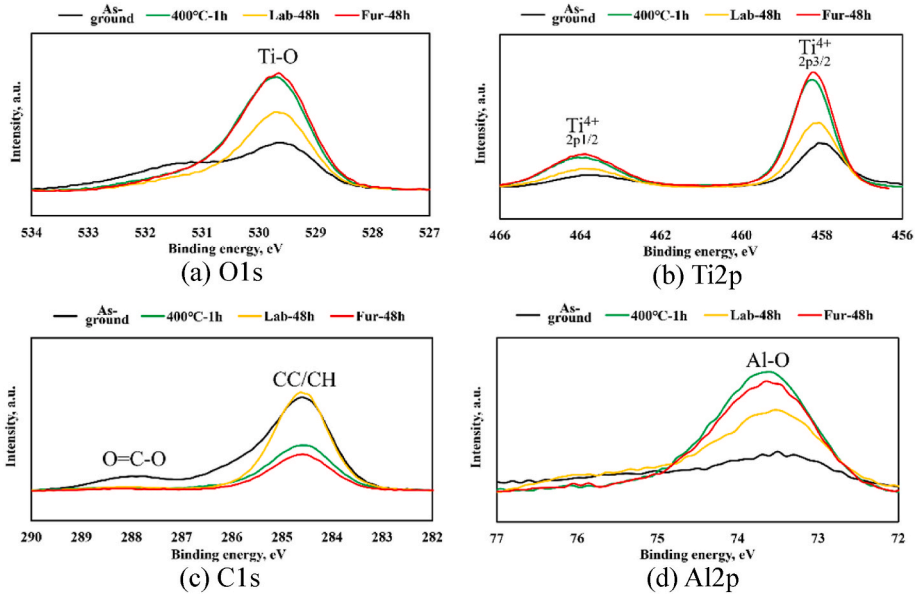

Fig. 17. XPS spectra after 48 h storage of Ti–6Al–4V heated at 400 °C for 1 h: (a) O1s, (b) Ti2p, (c) C1s, (d) Al2p; comparison of laboratory air vs. in-furnace (unopened) (Shift C1s 284.60eV).

(2) Heat treatment at 400–600 °C for 1 h yields high/ultra-high hydrophilicity together with a moderate oxide thickness; XPS shows strong Ti–O signals and low contamination. This window combines pronounced activation with a controllable film thickness and constitutes the principal contributor to bonding enhancement. Correspondingly, the 400°C–1h condition delivered the highest bonding performance, with an energy release rate of ~1455 J/m^2 by the DCB test.

(3) Excessive temperature is detrimental: at 800 °C, the outer layer becomes enriched in Al_2O_3 and markedly thickens; cracks tend to propagate within the brittle oxide layer (cohesive failure), rendering the adhesive joint nearly ineffective.

(4) Surface recontamination has a decisive impact on bonding performance. For the 400°C–1h condition, exposure to ordinary laboratory air rapidly causes re-hydrophobization and degrades *Gc* toward the untreated level; in contrast, closed-furnace storage (chamber unopened) effectively suppresses re-adsorption of adventitious carbon and associated recontamination, maintaining a low contact angle and higher *Gc*. The XPS analysis revealed that air-exposed samples show a renewed rise in C1s, whereas furnace-stored samples maintain largely stable surface chemistry, supporting that surface activation improves wettability and subsequently enhances the interface adhesive strength.

Consequently, the comprehensive results indicate that an effective condition for surface modification of Ti–6Al–4V is 400–600 °C for ~1 h, followed by immediate bonding before any recontamination. The findings provide practical guidance and a straightforward basis for the industrial implementation of heat treatment in adhesive bonding of Ti–6Al–4V structures.

Declaration of competing interest

The authors declare that they have no known competing financial interests or personal relationships that could have appeared to influence the work reported in this paper.

Acknowledgements

This work was supported by the Acquisition, Technology & Logistics Agency (ATLA) of Japan through the National Security Technology Research Promotion Program (JPJ004596) and by Japan Science and Technology Agency (JST) K Program, Japan (Grant Number JPMJKP24W1).The authors would like to express their gratitude to the Surface and Bulk Analysis Unit for the XRD measurements and to the Materials Forming Unit of NIMS Open Facility for sample preparation.

References

[1] Boyer RR. An overview on the use of titanium in the aerospace industry. Mater Sci Eng 1996;213:103–14. https://doi.org/10.1016/0921-5093(96)10233-1.
[2] Jensen LL, Bonnefoy PA, Hileman JI, Fitzgerald JT. The carbon dioxide challenge facing U.S. aviation and paths to achieve net zero emissions by 2050. Prog Aero Sci 2023;141:100921. https://doi.org/10.1016/j.paerosci.2023.100921.
[3] Westre WN, Olson JL, Schoeppner RL. Titanium-polymer hybrid laminates. United States patent US 2000;6. 114,050.
[4] Wang ZM, Ezugwu EO. Performance of PVD-coated carbide tools when machining Ti6Al4V. Tribol Trans 1997;40. https://doi.org/10.1080/10402009708983632. 81–86.
[5] Maressa P, Anodio L, Bernasconi A, Demir AG, Previtali B. Effect of surface texture on the adhesion performance of laser treated Ti6Al4V alloy. J Adhes 2014;91: 518–37. https://doi.org/10.1080/00218464.2014.933809.
[6] Bozkurt F, Çakır FH. An experimental design of spot welding of Ti6Al4V sheets and numerical modeling approach. Weld World 2021;65:885–98. https://doi.org/10.1007/s40194-020-01054-3.
[7] Baburaj EG, Starikov D, Evans J, Shafeev GA, Bensaoula A. Enhancement of adhesive joint strength by laser surface modification. Int J Adhesion Adhes 2007; 27:268–76. https://doi.org/10.1016/j.ijadhadh.2006.05.004.
[8] Yang W, Jin X, Luo Q, Li Q, Sun G. Adhesively bonded joints – a review on design, manufacturing, experiments, modeling and challenges. Compos B Eng 2024;276: 111225. https://doi.org/10.1016/j.compositesb.2024.111225.
[9] Molitor P, Barron V, Young T. Surface treatment of titanium for adhesive bonding to polymer composites: a review. Int J Adhesion Adhes 2001;21:129–36. https://doi.org/10.1016/S0143-7496(00)00044-0.
[10] Kim WS, Yun IH, Lee JJ, Jung HT. Evaluation of mechanical interlock effect on adhesion strength of polymer–metal interfaces using micro-patterned surface topography. Int J Adhesion Adhes 2010;30:408–17. https://doi.org/10.1016/j.ijadhadh.2010.05.004.
[11] Li J, Li Y, Huang M, Xiang Y, Liao Y. Improvement of aluminum lithium alloy adhesion performance based on sandblasting techniques. Int J Adhesion Adhes 2018;84:307–16. https://doi.org/10.1016/j.ijadhadh.2018.04.007.
[12] Yu Y-S, Xie L-S, Chen M-H, Wang N, Wang H. Surface characteristics and adhesive strength to epoxy of three different types of titanium alloys anodized in NaTESi electrolyte. Surf Coating Technol 2015;280:122–8. https://doi.org/10.1016/j.surfcoat.2015.09.010.
[13] Ardila-Rodríguez LA, Boshuizen B, Rans C, Poulis JA. The influence of grit blasting and UV/Ozone treatments on Ti–Ti adhesive bonds and their durability after sol–gel and primer application. Int J Adhesion Adhes 2021;104:102750. https://doi.org/10.1016/j.ijadhadh.2020.102750.

[14] Mertens T, Gammel FJ, Kolb M, Rohr O, Kotte L, Tschöcke S, et al. Investigation of surface pre-treatments for the structural bonding of titanium. Int J Adhesion Adhes 2012;34:46–54. https://doi.org/10.1016/j.ijadhadh.2011.12.007.
[15] Çakir FH. Enhancing the adhesive bonding strength of Ti6Al4V sheets with fiber laser texturing. Int J Adhesion Adhes 2022;114:103117. https://doi.org/10.1016/j.ijadhadh.2022.103117.
[16] Cheng F, Xu Y, Zhang J, Wang L, Zhang H, Wan Q, et al. Growing carbon nanotubes in-situ via chemical vapor deposition and resin pre-coating treatment on anodized Ti-6Al-4V titanium substrates for stronger adhesive bonding with carbon fiber composites. Surf Coating Technol 2023;457:129296. https://doi.org/10.1016/j.surfcoat.2023.129296.
[17] Liu Y, Su J, Tan C, Feng Z, Zhang H, Wu L, et al. Effect of laser texturing on mechanical strength and microstructural properties of hot-pressing joining of carbon fiber reinforced plastic to Ti6Al4V. J Manuf Process 2021;65:30–41. https://doi.org/10.1016/j.jmapro.2021.03.021.
[18] Tseng S-F, Chen Y-S. Surface microtexturing of Ti-6Al-4V and SS316L alloys using high pulsed fiber lasers for improving the adhesive bonded performance. Opt Laser Technol 2021;143:107349. https://doi.org/10.1016/j.optlastec.2021.107349.
[19] Rotella G, Orazi L, Alfano M, Candamano S, Gnilitskyi I. Innovative high-speed femtosecond laser nano-patterning for improved adhesive bonding of Ti6Al4V titanium alloy. CIRP J Manuf Sci Technol 2017;18:101–6. https://doi.org/10.1016/j.cirpj.2016.10.003.
[20] Melo Rodriguez G, Bowen J, Zelzer M, Stamboulis A. Selective modification of Ti6Al4V surfaces for biomedical applications. RSC Adv 2020;10:17642–52. https://doi.org/10.1039/c9ra11000c.
[21] Kasemo B, Lausmaa J. Biomaterial and implant surfaces: on the role of cleanliness, contamination, and preparation procedures. J Biomed Mater Res 1988;22(SA1):145–58. https://doi.org/10.1002/jbm.820221307.
[22] MacDonald DE, Rapuano BE, Deo N, Stranick M, Somasundaran P, Boskey AL. Thermal and chemical modification of titanium–aluminum–vanadium implant materials: effects on surface properties, glycoprotein adsorption, and MG63 cell attachment. Biomaterials 2004;25:3135–46. https://doi.org/10.1016/j.biomaterials.2003.10.029.
[23] García-Alonso MC, Saldaña L, Vallés G, González-Carrasco JL, González-Cabrero J, Martínez ME, et al. In vitro corrosion behaviour and osteoblast response of thermally oxidised Ti6Al4V alloy. Biomaterials 2003;24:19–26. https://doi.org/10.1016/S0142-9612(02)00237-5.
[24] Wang G, Li J, Lv K, Zhang W, Ding X, Yang G, et al. Surface thermal oxidation on titanium implants to enhance osteogenic activity and in vivo osseointegration. Sci Rep 2016;6:31769. https://doi.org/10.1038/srep31769.
[25] Hierro-Oliva M, Gallardo-Moreno AM, González-Martín ML. XPS analysis of Ti6Al4V oxidation under UHV conditions. Metall Mater Trans 2014;45:6285–90. https://doi.org/10.1007/s11661-014-2570-0.
[26] Li S, Lin J, Min J. Experimental investigation and molecular simulation on the chemical bonding between laser-treated titanium alloy amorphous surface and epoxy adhesive. J Adhes 2025;101(1):144–63. https://doi.org/10.1080/00218464.2023.2277298.
[27] SAE International. Titanium alloy, sheet, strip, and plate 6Al-4V annealed. AMS4911R 2019. https://doi.org/10.4271/AMS4911R [Internet]. [cited 2024 Dec 17].
[28] Guleryuz H, Cimenoglu H. Oxidation of Ti–6Al–4V and Ti–6Al–7Nb alloys. J Alloys Compd 2009;472(1–2):241–6. https://doi.org/10.1016/j.jallcom.2008.04.055.
[29] Pei X, Wu J, Xu Z, Li P. Analysis of high temperature oxidation process and mechanism of heterogeneous titanium alloy. Crystals 2025;15(9):810. https://doi.org/10.3390/cryst15090810.
[30] Diamanti MV, Del Curto B, Pedeferri MP. Interference colors of thin oxide layers on titanium. Color Res Appl 2008;33:221–8. https://doi.org/10.1002/col.20403.
[31] Gemelli E, Camargo NHA. Oxidation kinetics of commercially pure titanium. Rev Mater 2007;12(3):525–31. https://doi.org/10.1590/S1517-70762007000300014.
[32] ASM International. Titanium alloy Ti-6Al-4V – material data sheet. ASM Material Data Sheet. n.d. [Internet]. [cited 2025 Dec 12]. Available from: https://www.scribd.com/document/386833888/ASM-Material-Data-Sheet-Titanium-Alloy.
[33] Hay D, Fujita K, Fukumoto S. Effect of color change on composition and structure of anodized titanium. J Surf Eng Mater Adv Technol 2015;5:195–201. https://doi.org/10.4236/jsemat.2015.54020.
[34] Valentine MDA, Dhokia V, Flynn J, McNair SAM, Lunt AJG. Characterisation of residual stresses and oxides in titanium, nickel, and aluminium alloy additive manufacturing powders via synchrotron X-ray diffraction. Mater Today Commun 2023;35:105900. https://doi.org/10.1016/j.mtcomm.2023.105900.
[35] Diamanti MV, Pedeferri MP, Lorenzi M. Thermal oxidation of titanium: thin oxide film characteristics and growth kinetics. Thin Solid Films 2008;516(23):8523–9. https://doi.org/10.1016/j.tsf.2008.05.046.
[36] Boroushian M, Kosanovic T. Characterization of ultrathin oxide films on titanium using X-ray diffraction and XPS. Surf Coating Technol 2012;206(19–20):4108–13. https://doi.org/10.1016/j.surfcoat.2012.04.063.
[37] Masahashi N, Mizukoshi Y, Semboshi S, Ohtsu N. Superhydrophilicity of rutile TiO_2 prepared by anodic oxidation in high concentration sulfuric acid electrolyte. Chem Lett 2008;37:1126–7. https://doi.org/10.1246/cl.2008.1126.
[38] Maimaitiyili T, Woracek R, Neikter M, Boin M, Wimpory RC, Pederson R, et al. Residual lattice strain and phase distribution in Ti-6Al-4V produced by electron beam melting. Materials 2019;12(4):667. https://doi.org/10.3390/ma12040667.
[39] Carley AF, Chalker PR, Riviere JC, Roberts MW. The identification and characterization of mixed oxidation states at oxidised titanium surface by analysis of X-ray photoelectron spectra. J Chem Soc, Faraday Trans 1987;83:351–70.
[40] Wang Q, Song P, Niu W, Li N, Hu N. High temperature oxidation behavior of additive manufactured Ti6Al4V alloy with the addition of yttrium oxide nanoparticles. Materials 2024;17:2544. https://doi.org/10.3390/ma17112544.
[41] Mehrotra S, Kalyan D, Makineni SK, Santra S. Oxide growth characteristics, kinetics and mechanism of rutile formation on pure titanium. Vacuum 2024;219:112682. https://doi.org/10.1016/j.vacuum.2023.112682.
[42] Taira Y, Matsumura H, Yoshida K, Tanaka T, Atsuta M. Influence of surface oxidation of titanium on adhesion. J Dent 1998;26:69–73. https://doi.org/10.1016/S0300-5712(96)00072-3.
[43] Lee J-H, Ogawa T. The biological aging of titanium implants. Implant Dent 2012;21:415–21. https://doi.org/10.1097/ID.0b013e31826a51f4.
[44] Hamlekhan A, Butt A, Patel S, Royhman D, Takoudis C, Sukotjo C, et al. Fabrication of anti-aging TiO_2 nanotubes on biomedical Ti alloys. PLoS One 2014;9:e96213. https://doi.org/10.1371/journal.pone.0096213.